Large-scale slope instability at the southern margin of the Ediacaran Yangtze platform (Hunan province, central China)

E. Vernhet [a,b,*], C. Heubeck [b], M.-Y. Zhu [c], J.-M. Zhang [c]

[a] *Centre de Sédimentologie-Paléontologie, Université de Provence 3, Place Victor Hugo, 13331 Marseille-Cedex 3, France*
[b] *Institut für Geologische Wissenschaften, Freie Universität, Malteserstrasse 74-100, D-12249 Berlin, Germany*
[c] *Nanjing Institute of Geology and Palaeontology, 39 Beijing Donglu, Nanjing, 210008 Jiangsu Province, PR China*

Abstract

Thirteen stratigraphical sections from the Doushantuo Formation, Hunan province, central China, indicate large-scale mass wasting of the Yangtze platform margin between the late Neoproterozoic glaciation and the earliest Cambrian. Numerous sedimentary discontinuities, due to regional slides, olistostromes, and slumps have modified the stratigraphy between the shallow-water carbonate platform margin and the siliciclastic slope. Slide blocks are predominantly gently deformed and are largely composed of shallow water dolomitized limestones. Slide sheets may reach a regional extent of up to ~5000 km^2 and are embedded in anoxic shales at an unknown water depth.

1. Introduction

The Neoproterozoic and Cambrian strata of the Yangtze platform are one of the foremost locations in the world to study the Cambrian bioradiation. A detailed understanding of the temporal succession and ecological factors involved in this radiation event, however, has been hindered by the lack of detailed correlations between the numerous fossil-bearing locations and by a poor understanding of the depositional processes (Zhu et al., 2003). The transitional zone between the fossiliferous, stratigraphically incomplete, shallow-water carbonate environment and the stratigraphically complete but fossil free deepwater siliciclastic environment may enable a better correlation between the platform

and the basin. This would assist with reconstructing a detailed stratigraphical account of the tectonic and climatic drivers in the evolution of the Yangtze platform.

Thirteen stratigraphic sections were measured during two field seasons in 2002 and 2003. Representative samples were cut, polished, and scanned in order to highlight sedimentary structures and facies. Thin section petrography aided in the identification of mineralogy, diagenesis and microfacies. All sections are located in Hunan province, central China (Fig. 1), situated on the south-east facing slope of the Yangtze carbonate platform which formed during the Late Neoproterozoic (635-551 Ma) (Condon et al., 2005).

2. Geological setting

During the Late Neoproterozoic, the palaeogeographic location of South China and its position in the Rodinia supercontinent is, like many other small

---

* Corresponding author.
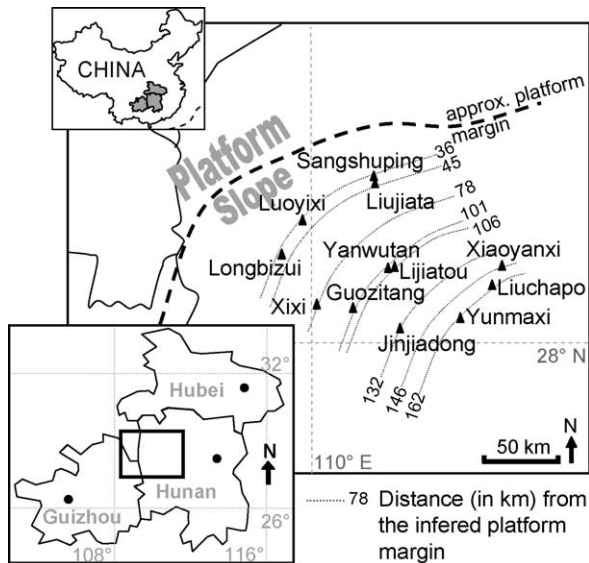 *E-mail address:* evernhet@up.univ-mrs.fr (E. Vernhet).

Fig. 1. Geographic location of the study area, northern Hunan Province, central China, representing the Ediacaran south eastward-dipping slope of the Yangtze platform.

blocks, poorly constrained. Li et al. (1995) proposed that the South China block linked Australia to Laurentia between 1 Ga and 700 Ma while Powell and Pisarevsky (2002) also joined South China to Australia in their reconstruction of Gondwana and Laurentia. Palaeomagnetic analyses suggest an equatorial location at 600 Ma (Macouin et al., 2004) with the collision of the Yangtze craton and the Cathaysia block (the south-eastern section of present-day China) forming the South China block during the Mesoproterozoic to early Neoproterozoic (Condie, 2003; Pisarevsky et al., 2003).

During the Neoproterozoic the Yangtze craton was located within an extensional regime following the break-up of Rodinia. After the Late Neoproterozoic the platform evolved into a passive continental margin (Wang and Li, 2003) (Fig. 2A.). Today the Yangtze craton is bordered by the Gingfeng–Xiangfan–Guangji (Qin-Lin) fault zone to the north, extending from Tibet to northern Anhui, and the Cathaysia suture to the southeast (Fig. 2B). This resulted from collisions with the Cathaysia block to the south-east during the Silurian and Early Triassic and the North China craton during the Early Triassic (Hsü and Chen, 1999). This caused a moderate deformation of the Palaeozoic sedimentary cover. Cretaceous extensional tectonics created large fault bounded basins filled by continental facies. In general, the Proterozoic–Palaeozoic strata are preserved at thickness of several kilometres and have been moderately deformed by large-scale folds.

2.1. Stratigraphy

Within the studied interval (Fig. 3) the sedimentary record is marked by diamictites in the Nantuo Formation, which are most likely a product of the Marinoan glaciation (Zhou et al., 2004; Condon et al., 2005). These putatively glaciogenic sediments have received renewed interest within the "Snowball Earth" theory (Hoffman et al., 1998; Hoffman and Schrag, 2000, 2002). A "cap carbonate" unit that overlies the tillites forms the base of the Doushantuo Formation. Unusual sedimentary structures (Nogueira et al., 2003) and a negative $\delta^{13}C$ isotope anomaly (Knoll et al., 1993; Germs, 1995; Corsetti and Hagadorn, 2000; Jiang et al., 2003) occur in these "cap carbonates", marking a sudden change from icehouse to greenhouse conditions during the Late Neoproterozoic. The diamictites of the Nantuo Formation and the overlying "cap carbonates" of the Doushantuo Formation occur widely throughout the central and southern Yangtze platform. The Doushantuo Formation in the Hunan province is dominated by black, thinly laminated, variably silicified shales inter-bedded with thin dark grey siltstone beds, which originate from turbidity currents, or occasionally with thinly laminated chert. Within this formation two phosphorite units are traceable across the region and are commonly used as stratigraphical markers. Tuffaceous sediments are common to abundant but are finely dispersed within the shales. The boundary of the Doushantuo Formation with the overlying Liuchapo Formation is conventionally placed at the first occurrence of the thick-bedded black chert. This boundary, though, is often eroded and in several sections represents the base of a major slide involving olistostromes and outcrop scale contorted bedding. The black silicified shales of the Liuchapo Formation grade updip into the dolomitized shallow-water limestones of the Dengying Formation, which are common across the platform in the northern Hunan and Hubei provinces.

3. Correlation of sections

Arranging the analysed sections according to their distance from the (inferred) margin of the shallow water, carbonate dominated, Yangtze platform (Figs. 1 and 4) indicates a progradational sequence containing numerous, laterally related, correlatable gravity deposits including slump folds, slides, olistostromes, debris flows and turbidites.

In the four sections closest to the inferred platform margin (between the Luoyixi and Liujiata sections) slump-folded shales are inter-bedded with gently
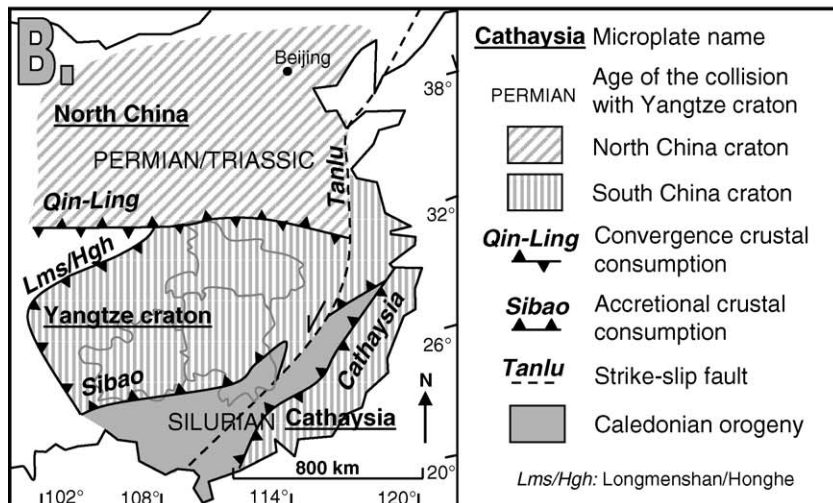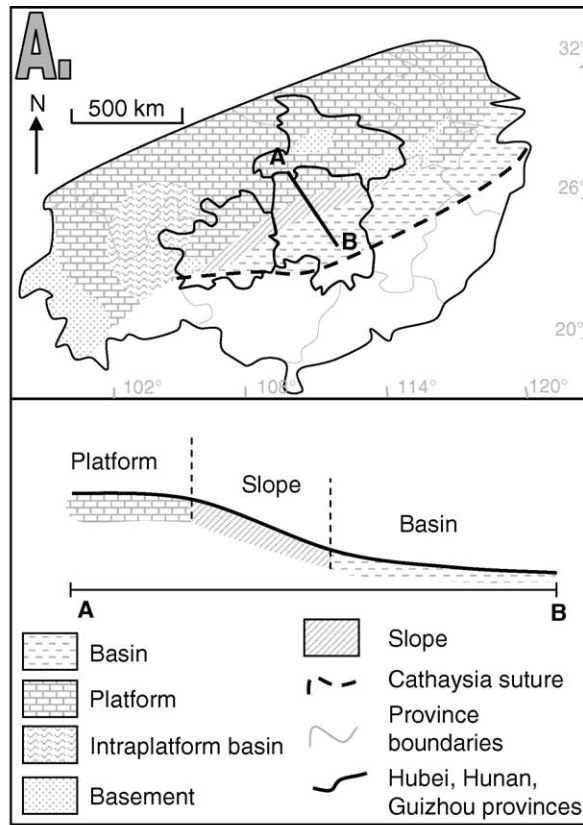
Fig. 2. (A) Palaeoenvironmental reconstruction of the southern Yangtze platform during the early Ediacaran (Doushantuo Fm; ∼635–550 Ma, Condon et al., 2005) (partly modified after Steiner, 2001). (B) Tectonic blocks of present-day eastern China. The North China block collided with Yangtze craton during the Permian/Triassic, while the Cathaysia block collided with Yangtze craton during the Silurian/Early Triassic. The Yangtze craton added the Cathaysia block to form the South China block (after Wang and Mo, 1995).

Fig. 3. Schematic stratigraphic column for the Ediacaran and basal Cambrian of central China.

deformed shallow water carbonates that range in thickness from 3 m (Luoyixi section, slide No. 4) to 25 m (Liujiata section, slide No. 2). The evaporites and phosphorites which overlay the laminated silty limestones in the No. 3 slide only occur at the Luoyixi section. Slide No. 3 attains its greatest thickness, ca. 45 m, in the six sections in the centrally located mid-slope region (between the Xixi and Jinjiadong sections). There adjacent, parautochthonous deformed, black shales and siltstones contain over a dozen olistoliths which range from several to tens of meters in diameter. As at the Luoyixi section the slide sheet at the Xixi section indicates basal evaporitic/phosphoritic lithologies overlain by laminated silty limestone (dark grey interval at the base of slide No. 3, Fig. 4). Slide sheet No. 3 in the Yanwutan section contains a poorly developed basal phosphorite interval overlain by ca. 40 m of grainstones/packstones and silty limestones. The equivalent of slide sheet No. 3 in the Jinjiadong section (54 km from the Xixi section) may be an olistostrome with meter-sized carbonate blocks. Finally, in the three most basinward sections (Yunmaxi to Xiaoyanxi sections), small scale folded and faulted, variably silicified black shales dominate the stratigraphical succession. Because of their equivalent stratigraphic position and the similarity in lithology and transport processes between the Luoyixi and Xixi sections for slide sheet No. 2 and the Luoyixi to Jinjiadong sections for slide sheet No. 3, the slide sheets and olistostromes identified by the shallow

water limestone facies can be correlated. The thickness of these units first increases and then decreases moving towards the basin (Fig. 4). At the Luoyixi section slide sheet No. 3 reaches 20 m in thickness whereas the same interval reaches 60 m 126 km downdip at the Yanwutan section. The allochthonous carbonate beds are, however, not exposed in the Longbizui section and do not appear in the basinal Liuchapo or Xiaoyanxi sections either. The contact between allochthonous carbonate slide blocks and underlying shales is always sharp and marked in well-exposed sections, such as the Xixi section, by a 5–10 cm thick unit of highly deformed scaly and fissile shales.

4. Description of olistostromes

Slide sheet sediments (e.g. slide No. 3 at the Xixi and Yanwutan sections (Fig. 4)) are internally folded into large-scale open folds tens of meters wide and several meters in amplitude. Unambiguous tight and isoclinal soft sedimentary slump folds, lacking foliation and showing plastic behaviour, deform the adjacent autochthonous or parautochthonous slope sediments. The base of the slide sheets is generally marked by a low angle contact with the underlying autochthonous shales, indicating the low erosive potential of the slide sheets. The orientation of the slump folds in the Luoyixi, Xixi, and Jinjiadong sections suggest a general North East to South West direction of transport (Fig. 5). The decimetre to metre scale carbonate olistoliths and discontinuity bounded carbonate intervals within the stratigraphic profiles are largely composed of shallow water carbonate platform lithologies (Vernhet, 2005).

In the outcrop three facies associations are distinguishable. Facies associations A and B represent allochthonous sediments whereas facies association C corresponds to autochthonous slope sediments. Facies analysis is summarized below and in Table 1.

4.1. Facies association A: low energy, shallow water environment

4.1.1. Description

Facies association A consists of two facies. Facies 1 is a thinly bedded dolomicrite inter-bedded with biolaminated patchy chert (Fig. 6A). These are deformed by "tepee" structures, which overlap the biolaminated chert beds. In thin sections facies 1 shows xenomorphous quartz crystals interrupting and deforming thin bituminous beds. Facies 2 consists of cm thick dolomicrite beds with convolute deformations and cm thick phosmicrite beds inter-bedded with very thin bedded microbreccia

Fig. 4. Stratigraphic correlation diagram between key sections in the Hunan province showing the south eastward-progradation of discrete mass slides (slides 1–4) on the south eastward-dipping slope of the Yangtze platform. See Fig. 1 for location.

Table 1
Summary of slope facies

| Facies association	Facies	Description	Components	Grain descriptions	Bedding type	Sedimentary structures	Interpretation	Sections
Allochthonous facies								
A	Facies 1	Biolaminated phosphorites, dolomicrite and/or patchy chert; locally, interbedded with fine-sized grainstones	Silica, phosphorite, evaporites	mm-Sized dolo- or phos-intraclasts; Stromatolitic clasts	~10 cm thick, laterally continuous, non-cyclic; lenticular bedding for the grainstones	Bio-laminations, desiccation structures as mudcracks and "tepees"	Edge of shallow-water in closed basin with emergence periods	Luoyixi, Yanwutan (Hunan)
	Facies 2	Phosmicrites with evaporitic dolomicrites; collapse and micro breccias	Apatite cement, dolomite micrites, evaporites	cm-to-dm-sized phos-intraclasts	Laterally discontinuous, lenticular bedding	Collapse breccias, evaporite-induced convolutes	Edge of shallow-water in closed basin with emergence periods	Xixi (Hunan)
B	Facies 3	Medium sand-sized wackestones/packstones with horizontal laminations or trough cross-bedding; locally, thin-bedded breccia	Intraclasts, carbonate micrite matrix, evaporite (?)	Medium sand-sized dolo-intraclasts; cm-sized phos-intraclasts in breccia	cm-to-dm-thick bedding, laterally continuous	Winnowing-induced horizontal laminations, cm-scale trough cross-bedding	Above fairweather wave base (~30 m water depth)	Xixi, Yanwutan, Luoyixi (Hunan)
	Facies 4–5	Cross-stratified grainstones/medium-sand-sized grainstones/packstones	Intraclasts, recrystallized dolomites, micrite	Medium sand-sized dolo-intraclasts	dm-Thick bedding, cross-strated, laterally discontinuous	Trough cross-bedding	Sandbanks (5–60 m water depth)	Yanwutan (Hunan)
Autochthonous facies								
C	Facies 6	Shales, shales interbedded with phosphorites and/or siltstones	(Calcareous) shales, apatite cement, (calcareous) siltstones		Thin-bedded, laterally continuous, non-cyclic	Thin parallel laminations due to discrete changes in grain size	Basin and slope with turbidite deposits	All sections
		Shales, mudstones, wackestones/packstones, slump folds, olistoliths	(Calcareous) shales, fine-grained sand wacke-stones/packstones; varying in olistoliths		Thin-bedded, laterally discontinuous, non-cyclic	Thin, plan-parallel laminations, slump folds, varying in olistoliths	Slope with turbidite deposits and olistostromes	Luoyixi, Longbizui, Xixi, Yanwutan, Sangshuping, Liujata, Jinjiadong, Liuchapo, Yunmaxi (Hunan)
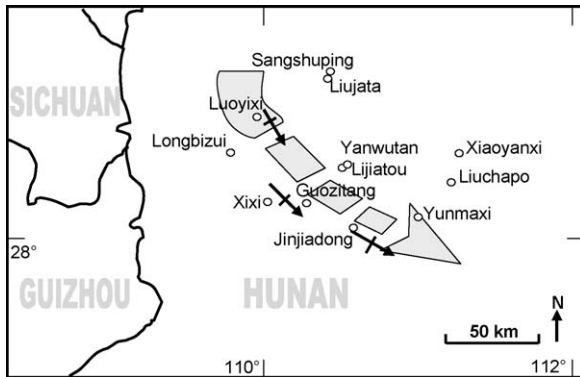
Fig. 5. Sediment transport direction, as inferred from the orientation of slump fold axes in three locations (Luoyixi, Xixi and Jianjiadong sections). Thin arrows point to downslope direction, perpendicular to axial plan of synsedimentary folds. Large grey arrow indicates overall direction of the mass wasting.

containing mm-sized phosphorite clasts (Fig. 6B) or dm-sized breccia with cm-sized phosphorite clasts (Fig. 6C). The phosmicrite is either a biolaminated brown-red phosmicrite ("soft" phosmicrite) or a black phosmicrite ("hard" phosmicrite). The dolomicrite shows different degrees of deformations, which affects the organisation of the phosmicrite bedding (Fig. 6C). In thin sections facies 2 reveals brown phosmicrite inter-bedded with bituminous rich beds and thin beds of euhedral dolomite crystals. Locally fan shaped crystals are also present.

4.1.2. Interpretation

The dominant micritic facies in facies association A suggest a low-energy environment. Rare high-energy events, such as storms, may have allowed the formation of microbreccias.

The "tepee" structures and the on-lapped chert beds observed in facies 1 may indicate that the sedimentation of the chert beds occurred after "tepee" formation. Consequently, "tepees" may represent syndeposition deformation following desiccation with facies 1 representative of deposition in a shallow water environment subjected to exposure periods.

The presence of evaporite in facies 2 is inferred from the convoluted structures and petrographic analysis of thin sections. Brecciation within facies 2 has resulted in the formation of evaporites, precipitation and dissolution, which may have induced a collapse of the phosphorite beds. The evaporites and micrites may either indicate a restricted evaporitic environment that was either located close enough to the platform margin to be incorporated into the slides, or was formed under early
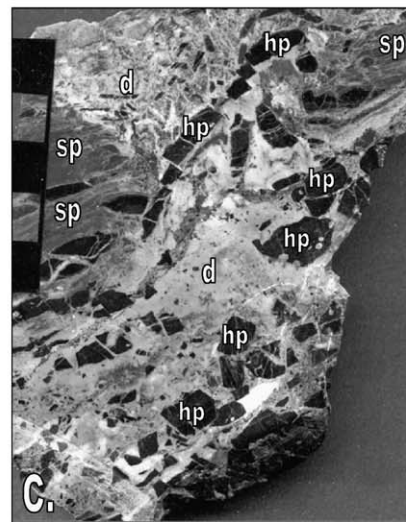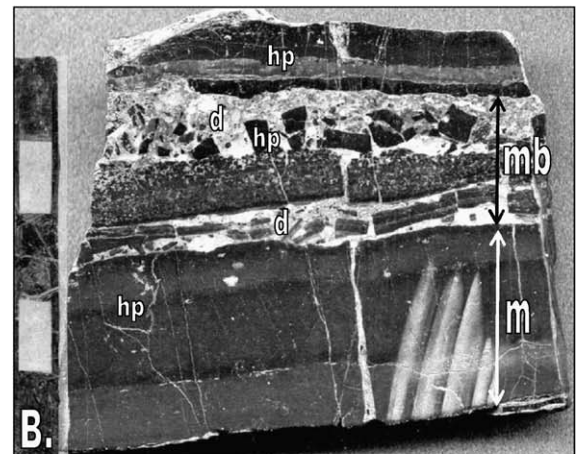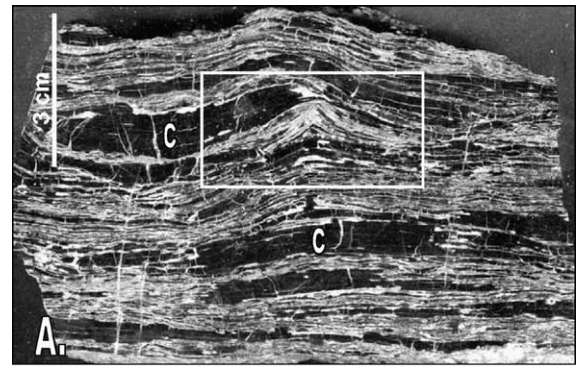

Fig. 6. Facies association A. Low-energy, shallow-water environment. (A) Facies 1: biolaminated patchy chert with "tepee" structures (white rectangle) inter-bedded with dolomite. Luoyixi section. (B) Facies 2: "hard" phosmicrite inter-bedded with microbreccia with mm-sized phosphorite clasts. Xixi section. (C) Facies 2: evaporite-mediated breccia. The formal presence of evaporite induced the collapse of the phosphorite beds by precipitation and dissolution. Xixi section. c: chert; d: dolomite; hp: "hard" phosphorite; sp: "soft" phosphorite; mb: microbreccia bed; m: phosmicrite bed. For (B) and (C) scale bar division = 1 cm.

diagenetic conditions with the oxidation of biogenic H_2S from decaying organic matter (Hill, 1995).

4.2. Facies association B: high-energy, shallow-water environment

4.2.1. Description

Facies association B consists of three facies represented by medium to high-energy deposits. Facies 3 includes packstones with mm-sized intraclasts organized in normally graded plan-parallel bedding surfaces and silty dolomitized limestones with trough, cm scale, cross-bedding (Fig. 7A). Facies 4 and 5 shows dm-sized trough cross-stratified and cross-bedded dolomitized limestones respectively (Fig. 7B). In thin sections these facies show euhedral to xenomorphous, ∼50 μm, dolomite crystals. Opaque minerals are rare.

4.2.2. Interpretation

The secondary dolomitization makes primary textures difficult to identify. The preserved sedimentary structures of these facies suggest that the dolomitized limestones were grainstones prior to dolomitization. However, the exact nature of grainstones (e.g., ooidal, peloidal) remains unknown. The normally graded, horizontally laminated, packstone and the trough cross-bedding which results in current ripples may indicate that facies 3 was deposited on a shallow water, wave dominated, subtidal shelf (Fig. 7A). The trough cross-stratified grainstones may originate from the displacement of sand banks (facies 4; Fig. 7B) while the dm-sized trough cross-bedding may correspond to the displacement of megaripples (facies 5). Consequently, these facies may also have been deposited on a shallow water subtidal shelf under the action of high-energy currents.

4.3. Facies association C: low-energy, deep-water environment

4.3.1. Description

Facies C is represented by thin-bedded silty shales inter-bedded with normally graded packstones/wackestones, rare thick bedded, grain-supported breccia/conglomerate (facies 6; Fig. 7C) showing internal soft-deformations, folded long angular clasts and cm- to dm-sized round clasts. Slump folds and discrete intra-formational discontinuities locally disturb the bedding in places (Fig. 7C).

4.3.2. Interpretation

Facies association C corresponds to the autochthonous and para-autochthonous sediments deposited on
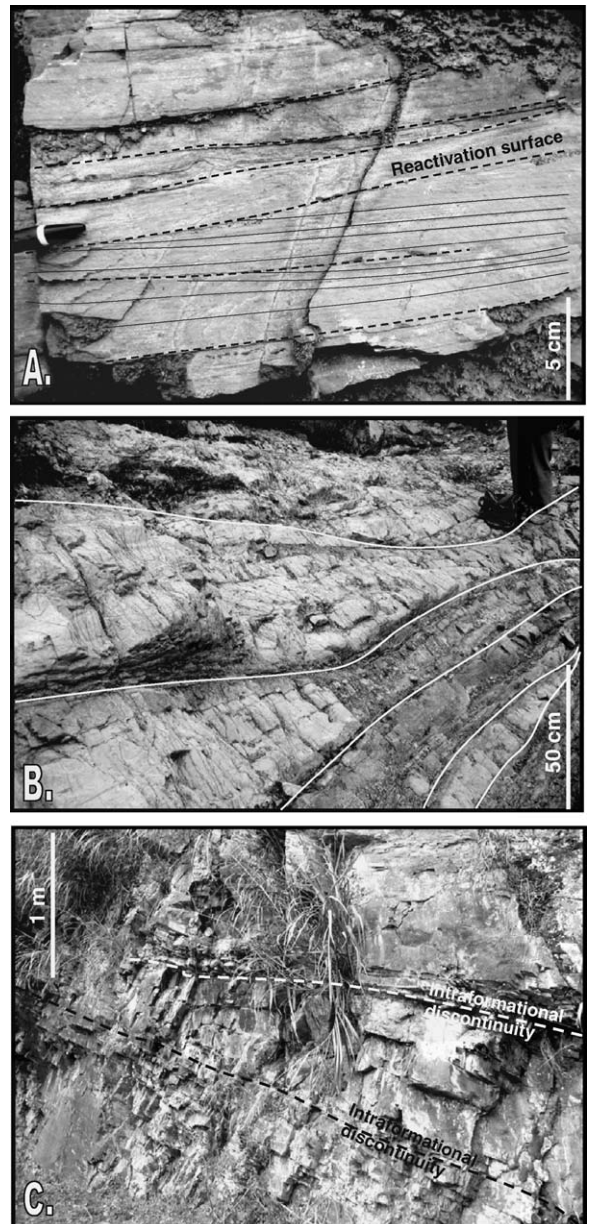

Fig. 7. Facies association B: high-energy, shallow water environment. (A) Trough cross-bedded silty limestones. Luoyixi section. (B) Trough cross-stratified grainstone. Yanwutan section. (C) Facies association C: low-energy, deep environment. Autochthonous black (silicified) shale. Discrete discontinuities correspond to the scar of previous slides.

the slope by suspension settling, or by turbiditic currents. Slump folds and discrete internal discontinuities also suggest that gravity-related mass movements have occurred. Breccia are interpreted as debrites resulting of debris flows.
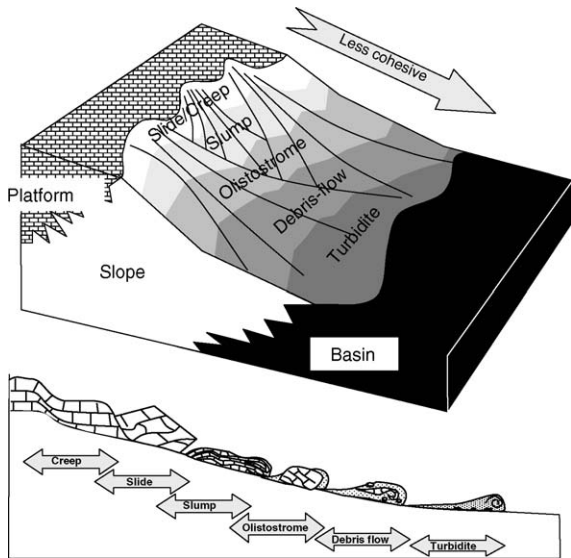
Fig. 8. Schematic ideal sequence of gravity induced facies occurring on submarine slopes (after Coniglio and Dix, 1992; Whitham, 1993; Stow et al., 1998; Lee and Chough, 2001).

5. Discussion

5.1. Evidence of large-scale mass displacements

Three criteria serve to identify large-scale slides: The laterally correlated units reveal the general characteristics of gravity movement processes in a logical downdip succession and may include the complete spectrum of mass displacement processes (Fig. 8). During the initiation of mass movements slumps and slides create gently folded limestones (Fig. 9A and A′) above discrete levels of highly deformed basal shear (Coniglio and Dix, 1992), megatruncation surfaces (Stewart et al., 1993) and slip surfaces (Stow et al., 1998) (Fig. 9B and C). Within mass movements slides of decametre thickness and possible km scale lateral extent and olistostromes involving meter-sized blocks increase in abundance (Fig. 9D). At the end of the mass movement the reduction in olistolith size (Jinjiadong section) or their absence in downslope sections (Liuchapo and Xiaoyanxi sections) indicates that olistostromes were replaced by debrites (Fig. 9E) or turbidites. Meter-scale tight to isoclinal slump folds are common throughout the study area allowing the downslope transportation direction to be inferred.

The complete theoretical sequence of gravity related deformations (Fig. 8) cannot be identified in a single slide sheet. Slide sheet No. 1 (Fig. 4) shows only debrite (Fig. 9E) while slide sheet No. 4 (Fig. 4) shows only olistostromes (Fig. 9D). Except for the debrites of slide sheet No. 1 (Fig. 4), the cohesion of the olistolith sediments in the large-scale olistostromes (slide sheets No. 2, 3, and 4; Fig. 4) are preserved and may represent an early stage of mass movement.

Abrupt and erosional contacts in the stratigraphic profiles without transitional facies from deep-water (autochthonous) facies to shallow water (allochthonous) facies are present throughout. Slide units include facies deposited in shallow-water protected basins with periods of exposure (facies association A; facies 1 and 2) and facies deposited on the shallow water, subtidal, wave-dominated platform (facies association B; facies 3, 4, and 5). The presence of these facies, which are unexpected in slope environments, supports an allochthonous origin for these deposits and the large-scale slide sheet interpretations detailed above.

These unusual facies successions have a regional coverage. The allochthonous shallow water carbonates are present within a single stratigraphic unit for at least 70 km between the Luoyixi and Yanwutan sections. This may represent either an assemblage of individual blocks exceeding outcrop size (several 100 m) at each of the three adjacent mid-slope locations for the Liujiata, Xixi and Yanwutan sections or, a single coherent body on the mid slope of ca. 50 km × 70 km in size.

5.2. Slide dimensions, displacement distance, and slope geometry

The largest, recent, documented submarine slides are from the volcanic flanks of Hawaii (Moore et al., 1995; Cervelli et al., 2002; Ward, 2002) and Tenerife (Hürlimann et al., 2001). Some of these slides consist of up to 2000 km³ of re-mobilized sediment (Ward, 2002). Debrites and turbidites, the most distal deposits of mass wasting, may be transported up to several hundred kilometres from their source (Coniglio and Dix, 1992). These processes have been studied using seismic data and sonar imagery along modern slopes. For example, the recent Palos Verdes, California, slide carried ca. 0.34 km³ of mass sediment over 4–5 km (Bohannon and Gardner, 2004). In the North Aegean Sea Lykousis et al. (2002) documented a slide of 3–8 km³ over an area of 85 km² and a runout distance of 6–7 km. In the Japanese Sea Lee et al. (1996) studied slide sheets 10 km long and 50 m thick. The geological record also preserves examples of significantly larger slides. Beutner and Craven (1996) describe a coherent Ordovician carbonate mass movement of 1300 km² and several kilometres thickness that moved 30 km along a gently dipping surface. Similarly, Stewart et al. (1993) documented truncation surfaces over 56 km along the depositional strike and 8 km basin-
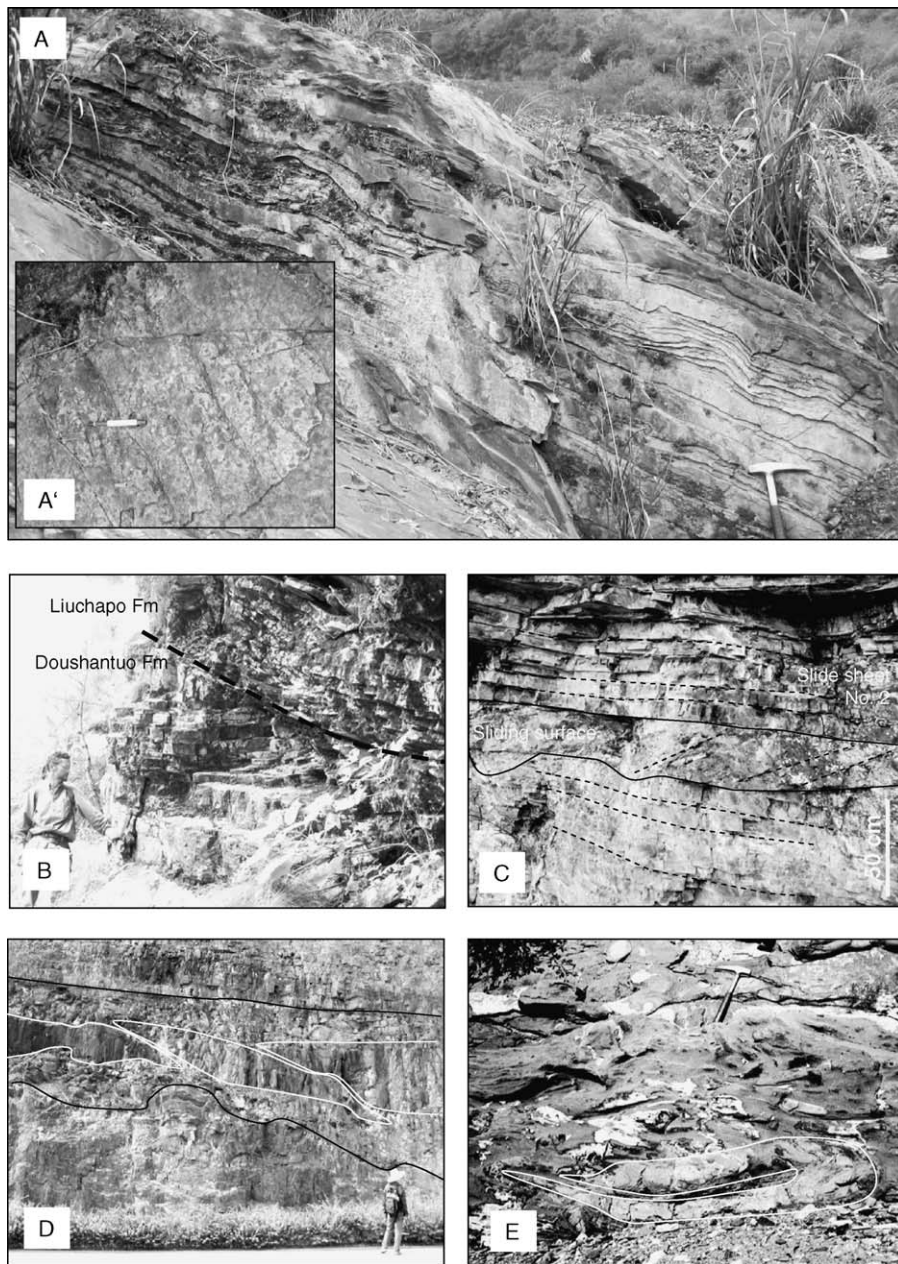
Fig. 9. (A) Gravity-related deformations in the silty limestones of slide sheet No. 3 at Xixi section. (A′) cm-sized ripples on the surface bedding of the silty limestones in slide sheet No. 3 (Xixi section). (B) Angular discontinuity between the Doushantuo Formation shales and overlying black silicified shales of the Liuchapo Formation, representing a slide horizon (Jinjiadong section). (C) Highly deformed sediment interval interpreted as the slide surface at the base of slide sheet No. 2 (Xixi section, lower Doushantuo Formation). (D) Elongate silty limestone olistoliths (slide sheet No. 4, white lines) in dm to m scale, slump folded black shale (upper Doushantuo Formation in the Luoyixi section). Note the erosive base of the olistolith and the undeformed overlying beds (black lines). (E) Debrites, showing near complete loss of sediment cohesion and local plastic deformation, folded bed (white contour) (Sangshuping section, slide sheet No. 1).

ward. Large-scale submarine sliding or gravity induced mass movement can occur along detachment surfaces due to reduced frictional strength. This may be caused by high pore-water pressure (Spence and Tucker, 1997; Huvenne et al., 2002; Lykousis et al., 2002; Watts, 2004; Martel, 2004), the dissociation of gas hydrates (Lee et al., 1996) or by the injection of volcanic gases (Beutner and Craven, 1996).

The approximate location of the Yangtze platform margin can be constrained from existing data (Bureau

of Geology and Mineral Resources, 1987, 1988, 1990) (Fig. 1). The greatest updip and proximal part of slide No. 3 (Luoyixi section) appears to be located approximately 36 km basinward of the inferred platform margin (Figs. 1 and 4). Fragmentation of this slide sheet occurs approximately 130 km basinward of the platform margin, upslope of the Jinjiadong section (Fig. 10). Therefore, this slide is estimated to cover an area of approximately 5000 km^2 with a minimum thickness of about 10 m. The volume of displaced sediments probably

exceeds 50 km^3. Thus, the large-scale slide sheet No. 3 in the Ediacaran Yangtze platform slope, compared with previously studied major slides, shows an unusual large-scale extent area and small thickness.

Earthquakes (Mullins et al., 1991; Heubeck, 1992; Hürlimann et al., 2001), previous stress history (Silva et al., 2004), intense storm events (Stow et al., 1998), significant regressions (Lee et al., 1996, Spence and Tucker, 1997) or sediment overloading (Coniglio and Dix, 1992; Bosellini et al., 1993; Spence and Tucker, 1997) may
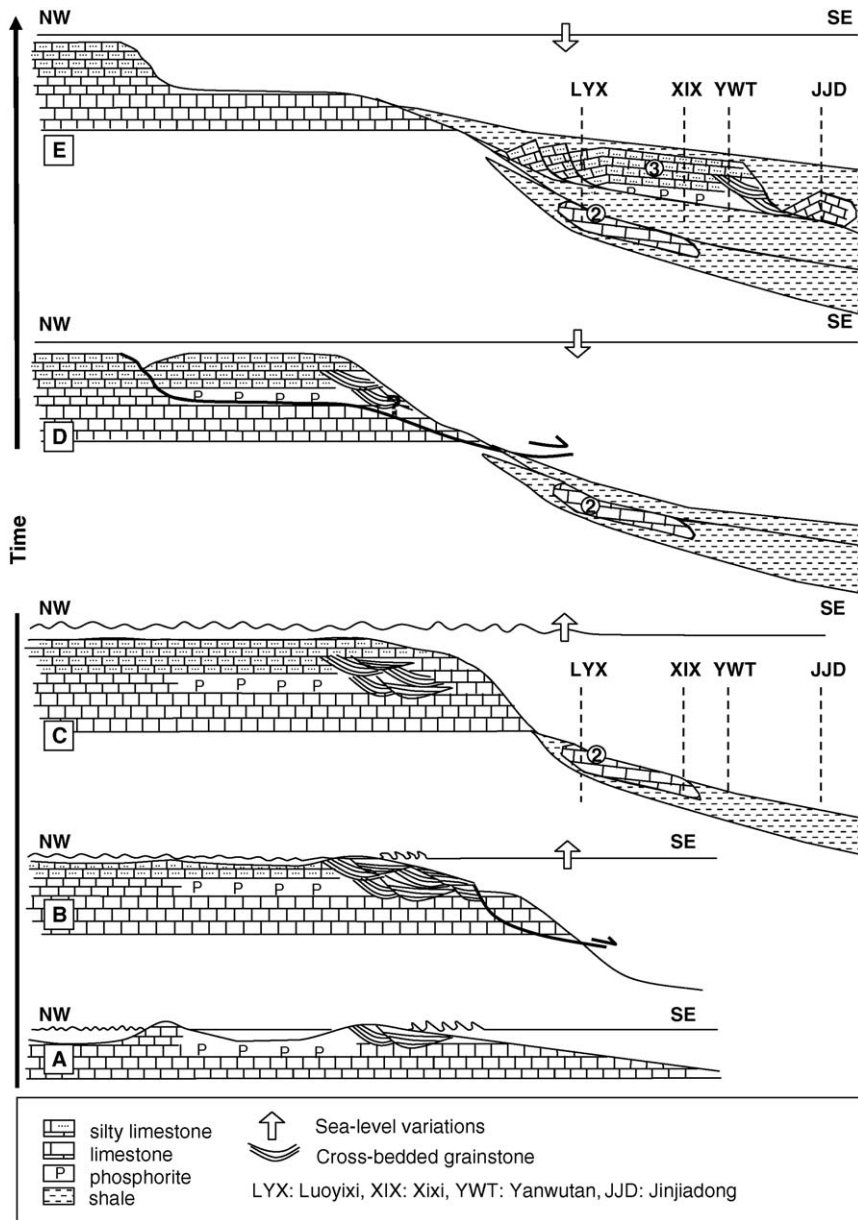

Fig. 10. Proposed sedimentary evolution for the allochthonous deposits on the Ediacaran south eastward-dipping Yangtze platform.

have initiated this sliding. The presence of evaporites and phosphorites at the base of several large-scale slides may have facilitated this displacement.

A relationship between large scale mass wasting along the platform margin and variations in sea level may also exist. The internal stratigraphy of the largest slide block, No. 3, consists of a phosphoritic and evaporitic interval with exposure features overlain by a medium to coarse-grained carbonate interval. These may reflect a sea level lowstand facies overlain by a transgressive or sea level highstand facies. Based on similarities within the lithological sequence and its thickness and facies, Vernhet (2005) proposed a correlation between the internal slide sheet stratigraphy and autochthonous sections of the Doushantuo Formation. A subsequent lowstand, not represented in the slide sheet No. 3, may have triggered widespread mass wasting along the southeast-facing platform.

6. Conclusions

Our work documents large-scale mass transportation on the Yangtze platform slope during the Ediacaran. Three criteria help to identify the oversized slide sheets: (1) correlation between sections of allochthonous intervals; (2) abrupt vertical facies changes separated by thin, highly deformed, beds: interpreted as displacement levels; (3) the regional extent of the sliding unit. The sedimentary facies of the slide blocks allows an approximate reconstruction of the platform margin, which primarily consists of shallow water more or less restricted environment. Displacement may have been facilitated by the presence of low strength evaporites and brittle phosphorites at the base of the slides and/or by water and gas accumulation in the highly stratified sediments. Geochemical profiles in the deep-water facies of the Doushantuo Formation, aiming at sampling stratigraphically continuous sections of the Ediacaran, need to take into account the stratigraphic complexities caused by these widespread mass wasting events.

Acknowledgements

References

Beutner, E.C., Craven, A.E., 1996. Volcanic fluidization and the Heart Mountain detachment, Wyoming. Geology 24, 595–598.

Bohannon, R.G., Gardner, J., 2004. Submarine landslides of San-Pedro escarpment, southwest of Long Beach, California. Mar. Geol. 203, 261–268.

Bosellini, A., Neri, C., Luciani, V., 1993. Platform margin col-lapses and sequence stratigraphic organization of carbonate slopes: Cretaceous-Eocene, Gargano Promontory, southern Italy. Terra Nova 5, 282–297.

Bureau of Geology and Mineral Resources of Guizhou Province, 1987. Regional Geology of Guizhou Province, Geological Mem-oirs Series 1 Number 7. Geological Publishing House, Beijing.

Bureau of Geology and Mineral Resources of Hunan Province, 1988. Regional Geology of Hunan Province, Geological Memoirs Series 1 Number 8. Geological Publishing House, Beijing.

Bureau of Geology and Mineral Resources of Hubei Province, 1990. Regional Geology of Hubei Province, Geological Memoirs Series 1 Number 20. Geological Publishing House, Beijing.

Cervelli, P., Segall, P., Johnson, K., Lisowski, M., Miklius, A., 2002. Sudden aseismic fault slip on the south flank of Kilauea volcano. Nature 415, 1014–1018.

Condie, K.C., 2003. Supercontinents, superplumes and continental growth: the Neoproterozoic record. In: Windley, Y.M., Dasgupta, S., Yoshida, M. (Eds.), Proterozoic East Gondwana: Supercontinent Assembly and Breakup. Geol. Soc. Publ. House, London.

Condon, D., Zhu, M.-Y., Bowring, S., Yang, A., Jin, Y.-G., 2005. U-Pb ages from the Neoproterozoic Doushantuo Formation, China. Science 308, 95–98.

Coniglio, M., Dix, G.R., 1992. Carbonate slopes. In: Walker, R.G., James, N.P. (Eds.), Facies Models: Responses to the Sea Level Change. Geol. Soc., Canada.

Corsetti, F.A., Hagadorn, J.W., 2000. Precambrian-Cambrian transi-tion: Death Valley, US. Geology 28, 299–302.

Germs, G.J.B., 1995. The Neoproterozoic of southwestern Africa, with emphasis on platform stratigraphy and paleontology. Precambrian Res. 73, 137–151.

Heubeck, C., 1992. Sedimentology of large olistoliths, southern Cordillera Central, Hispaniola. J. Sed. Petrol. 62, 474–482.

Hill, C., 1995. Sulfur redox reactions: hydrocarbons, native sulfur, Mississippi Valley-type deposits, and sulfuric acid karst in the Delaware Basin, New Mexico and Texas. Environ. Geol. 25, 16–23.

Hoffman, P.F., Kaufman, A.J., Halverson, G.P., Schrag, D.P., 1998. A Neoproterozoic snowball earth. Science 281, 1342–1346.

Hoffman, P.F., Schrag, D.P., 2000. Snowball earth. Sci. Am. 282, 68–76.

Hoffman, P.F., Schrag, D.P., 2002. The snowball earth hypothesis: test-ing the limits of global change. Terra Nova 14, 129–155.

Huvenne, V.A.I., Crocker, P.F., Henriet, J.-P., 2002. A refreshing 3D view of an ancient sediment collapse and slope failure. Terra Nova 14, 33–40.

Hürlimann, M., Ledesma, A., Martí, J., 2001. Characterisation of a volcanic residual soil and its implications for large landslide phe-nomena: application to Tenerife, Canary Islands. Eng. Geol. 59, 115–132.

Hsü, K.J.H., Chen, H.-H., 1999. Geologic Atlas of China. Elsevier, Amsterdam.

Jiang, G.-Q., Kennedy, M.J., Christie-Blick, N., 2003. Stable isotopic evidence for methane seeps in Neoproterozoic postglacial cap carbonates. Nature 426, 822–826.

Knoll, A., Fairchild, I.J., Swett, K., 1993. Calcified microbes in Neoproterozoic carbonates: implications for our understanding of the Proterozoic/Cambrian transition. Palaios 8, 512–525.

Lee, H.J., Chough, S.K., Yoon, S.H., 1996. Slope-stability change from late Pleistocene to Holocene in the Ulleung Basin, East Sea (Japan). Sed. Geol. 104, 39–51.

Lee, S.H., Chough, S.K., 2001. High-resolution (2–7 kHz) acoustic and geometric characters of submarine creep deposits in the South Korea Plateau, East Sea. Sedimentology 48, 629–644.

Li, Z.-X., Zhang, L., McA-Powell, C., 1995. South China in Rodinia: part of the missing link between Australia—East Antarctica and Laurentia? Geology 23, 407–410.

Lykousis, V., Roussaki, G., Alexandri, M., Pavlaki, P., Papoulia, I., 2002. Sliding and regional slope stability in active margins: North Aegean Trough (Mediterranean). Mar. Geol. 186, 281–298.

Macouin, M., Besse, J., Ader, M., Gilder, S., Yang, Z., Sun, Z., Agrinier, P., 2004. Combined paleomagnetic and isotopic data from the Doushantuo carbonates, South China: implications for the "snowball Earth" hypothesis. Earth Planet. Sci. Lett. 224, 387–398.

Martel, S.J., 2004. Mechanics of landslide initiation as a shear fracture phenomenon. Mar. Geol. 203, 319–339.

Moore, J.G., Bryan, W.B., Beeson, M.H., Normark, W.R., 1995. Giant blocks in the South Kona landslide, Hawaii. Geology 23, 125–128.

Mullins, H.T., Dolan, J., Breen, N., Andersen, B., Gaylord, M., Petruccione, J.L., Wellner, R.W., Melillo, A.J., Jurgens, A.D., 1991. Retreat of carbonate platforms: response to tectonic processes. Geology 19, 1089–1092.

Nogueira, A.C.R., Riccomini, C., Nóbrega Sial, A., Veloso Moura, C.A., Fairchild, T.R., 2003. Soft-sediment deformation at the base of the Neoproterozoic Puga cap carbonate (SW Amazon craton, Brazil): confirmation of rapid icehouse to greenhouse transition in Snowball Earth. Geology 31, 613–616.

Pisarevsky, S.A., Wingate, M.T.D., McA Powell, C., Johnson, S., Evans, D.D., 2003. Models of Rodinia assembly and fragmentation. In: Windley, Y.M., Dasgupta, S., Yoshida, M. (Eds.), Proterozoic East Gondwana: Supercontinent Assembly and Breakup. Geol. Soc. Publ. House, London.

Powell, C.M., Pisarevsky, S.A., 2002. Late Neoproterozoic assembly of East Gondwana. Geology 30, 3–6.

Silva, A.J., Baxter, C.D.P., LaRosa, P.T., Bryant, W.R., 2004. Investigation of mass wasting on the continental slope and rise. Mar. Geol. 203, 355–366.

Spence, G.H., Tucker, M.E., 1997. Genesis of limestone megabreccias and their significance in carbonate sequence stratigraphic models: a review. Sediment. Geol. 112, 163–193.

Steiner, M., 2001. Die fazielle Entwicklung und Fosiilverbreitung auf der Yangtze Plattform (Südchina) im eoproterozoikum/frühesten Kambrium. Freiberger Forschungshefte 492, 1–26 (in German).

Stewart, W.D., Dixon, O.A., Rust, B.R., 1993. Middle Cambrian carbonate-platform collapse, southeastern Canadian Rocky Mountains. Geology 21, 687–690.

Stow, D.A.V., Reading, H.G., Collinson, J.D., 1998. Deep seas. In: Reading, H.G. (Ed.), Sedimentary Environments: Processes, Facies and Stratigraphy. Blackwell, Oxford.

Vernhet, E., 2005. Sedimentary processes, evolution, and paleoenvironmental reconstruction of the southern margin of the Ediacaran Yangtze platform (Doushantuo Formation, central China). PhD Thesis, Freie Universität Berlin, 175 pp.

Wang, H.-Z., Mo, X.-X., 1995. An outline of the tectonic evolution of China. Episodes 18, 6–16.

Wang, J., Li, Z.X., 2003. History of the Neoproterozoic rift basins in South China: implications for Rodinia break-up. Precambrian Res. 122, 141–158.

Ward, S.N., 2002. Slip-sliding away. Nature 415, 973–974.

Watts, P., 2004. Probabilistic predictions of landslide tsunamis off Southern California. Mar. Geol. 203, 281–301.

Whitham, A.G., 1993. Facies and depositional processes in an Upper Jurassic to Lower Cretaceous pelagic sedimentary sequence, Antarctica. Sedimentology 40, 331–349.

Zhou, C.-M., Tucker, R., Xiao, S.-H., Peng, Z.-X., Yuan, X.-L., Chen, Z., 2004. New constraints on the ages of Neoproterozoic glaciations in south China. Geology 32, 437–440.

Zhu, M.-Y., Zhang, J.-M., Steiner, M., Yang, A.-H., Li, G.-X., Erdtmann, B.D., 2003. Sinian and Early Cambrian stratigraphic frameworks from shallow- to deep-water facies of the Yangtze Platform: an integrated approach. Prog. Nat. Sci. 13 (12), 951–960.